This manuscript is a preprint and has been submitted for publication in *Nature Communications*. The manuscript has yet to be formally accepted for publication. Subsequent versions of this manuscript may have slightly different content. If accepted, the final version of this manuscript will be available via the 'Peer-reviewed Publication DOI' link on the right-hand side of this webpage.

Please feel free to contact any of the authors; we welcome feedback.

# Distributed sensing of earthquakes and ocean-solid Earth interactions on seafloor telecom cables

A. Sladen[1], D. Rivet[1], J.P Ampuero[1], L. De Barros[1], Y. Hello[1], G. Calbris[2], P. Lamare[3]

[1] Université Côte d'Azur, CNRS, Observatoire de la Côte d'Azur, IRD, Géoazur, 250 rue Albert Einstein, Sophia Antipolis 06560 Valbonne, France
[2] Febus-optics, Technopole Helioparc - 2 av. Président Pierre Angot - 64 000 Pau – France
[3] Aix Marseille Univ, CNRS/IN2P3, CPPM, Marseille, France

***Abstract***

Two thirds of the surface of our planet are covered by water and are still poorly instrumented, which has prevented the earth science community from addressing numerous key scientific questions. The potential to leverage the existing fiber optic seafloor telecom cables that criss-cross the oceans, by turning them into dense arrays of seismo-acoustic sensors, remains to be evaluated. Here, we report Distributed Acoustic Sensing measurements on a 41.5 km-long telecom cable that is deployed offshore Toulon, France. Our observations demonstrate the capability to monitor with unprecedented details the ocean-solid earth interactions from the coast to the abyssal plain, in addition to regional seismicity (e.g., a magnitude 1.9 micro-earthquake located 100 km away) with signal characteristics comparable to those of a coastal seismic station.

## Article

About 70% of the Earth's surface is covered by oceans, thus barely accessible to *in situ* instrumentation and opaque to remote sensing. Paradoxically, our vision of the geologic and biologic richness of the oceans, a not-so-distant world, remains fragmentary. The challenge of instrumenting the oceans is tantalizing as it holds the answers to numerous fundamental scientific questions, such as the dynamics of the oceans, the internal structure of the Earth, and the complex interaction between life, geology and oceans. This challenge also encompasses the monitoring of various natural resources and natural hazards (earthquakes, tsunamis, submarine landslides), including those in coastal areas that are increasingly vulnerable in a changing climate.

Adapting instrumentation to the extreme conditions of the ocean floor (pressure, biofouling, corrosion) requires expertise and is costly, with the main hurdle being the cost of ship time for deployment and recovery. Drifting sensors, such as the Argo and Mermaid floats (*1*, *2*), can rapidly cover large areas, but remain limited by satellite transmission, power supply and

poor control over sensor locations. Permanent seafloor observatories for long-term monitoring(*3*), comprised of multi-physics platforms connected to land by an electro-optic cable, are very costly to install and maintain(*4*), which limits their spatial extent, density and scope. While these different approaches have enabled significant discoveries and will continue to benefit science and society, our vision of the 3D water world and what lies below remains limited to mere glimpses.

Owing to the rise of the internet, most oceans are crossed by fiber optic cables that present the possibility to leverage this infrastructure for scientific purposes (*5*). Recognizing this opportunity, an International Joint Task Force was established in 2012 to design "SMART" (Scientific Monitoring And Reliable Telecommunications) cables with environmental sensors embedded in repeater boxes placed approximately every 50 km (*6*). Recently, the capacity to turn optical fibers (OF) into seismo-acoustic sensors has been developed. One breakthrough was the coincidental discovery that earthquakes can be detected by analyzing the phase stability of state-of-the-art lasers across thousand-kilometer-long seafloor telecommunication cables(*7*). Yet, this approach only provides one measurement, which is integrated over the entire length of the cable. An alternative approach, called Distributed Acoustic Sensing (DAS), exploits the phase of light that is back-scattered by the inherent inhomogeneities of the silica fiber to provide densely spaced, high-rate measurements of strain. DAS can provide high frequency (1 kHz) acoustic measurements with metric spacing, effectively turning OF cables into dense linear seismic arrays(*8*). The technology has been used in the oil and gas industry for many years now, but has only recently revealed its full potential for seismological and environmental applications(*9–12*). DAS on seafloor telecom cables is not as straightforward as it might initially seem, because these are sturdy cables with jelly compound layers and metallic armoring. These barriers are designed to provide stability and protection from torsion and external disruptions, most notably by fishing activities in coastal areas (*13*). Additionally, weak coupling between the cable and the poorly consolidated sediments on the seafloor may prevent accurate recording of seismic waves. The performance of DAS on submarine telecom cables therefore remains to be demonstrated. To address this gap, here we present results of DAS measurements performed on such a cable. We show that the measurements are indeed highly sensitive to seismo-acoustic signals, and that such cables can readily provide continuous, dense measurements over large distances to study a range of marine and solid-earth phenomena with unprecedented levels of detail.

Data were acquired from February 19th to February 24th, 2018, on a 41.5 km-long electro-optic telecommunication cable from Alcatel, which is deployed offshore Toulon in the south of France. This cable is the backbone of the MEUST-NUMerEnv project(*14*) (Mediterranean Eurocentre for Underwater Sciences and Technologies - Neutrino Mer Environnement). The cable straddles several oceanic domains of the north Mediterranean margin: a shallow continental shelf, a steep continental slope, and a 2500 m-deep oceanic plain. The main purpose of the cable is to collect data from the KM3NeT/ORCA (Oscillation Research with Cosmics in the Abyss) neutrino detector deployed at its seafloor termination point (*15*). The MEUST cable was installed in 2014 (*16*) and, as is often the case with

telecommunication cable, was simply laid on the seafloor. The cable is only buried for the first 2 km offshore (see supplementary material for details of the cable installation).

The DAS interrogator unit is connected to one end of the fibers. Coherent pulses of light are emitted through the OF and phase changes of the backscattered light signal are continuously recorded. Local dilatation and contraction between two locations of the fiber induced by environmental seismic perturbation cause linear phase changes of the reflected back-scattered signals allowing to measure associated strain or strain-rate in the longitudinal (*17*). The distance between two phase change measurements is called the gauge length and a measurement consists in the integration of the perturbation along the gauge length. In most cases, a better signal to noise ratio is obtained for a longer gauge length but it needs to stay smaller than the shorter acoustic wavelengths targeted. In our experiment, the gauge length was fixed to 19.2 m. The dataset used in this study consists of strain rate value sampled every 6.4 m in space and 0.5 ms in time yielding about 6500 acoustic sensors with an effective recording frequency of 1 kHz.

Along its entire length, the OF cable continuously records a background signal made of periodic oscillations. These oscillations have different properties on the continental shelf and on the abyssal plain. We describe them sequentially hereafter, starting with observations near the coast.

The signals in the first 8 km of underwater cable are dominated by periodic oscillations with frequencies between 0.1 and 0.25 Hz, which propagate landward with increasing amplitude (Fig. 2B,C). Their amplitude decays rapidly with depth as predicted by the linear theory of gravity waves in a water layer of finite thickness *h*:

$$\frac{P_d(h)}{P_{d0}} = \frac{1}{\cosh\,(k.h)}$$

with $P_d(h)$ and $P_{d0}$ being the dynamic pressure at the seafloor and at the surface, respectively, and k being the wavenumber. The OF cable senses the dynamic pressure produced by the surface gravity wave down to a depth of 100 m, close to the lower limit of wave action, where amplitudes as low as 1 nstrain/s are measured. The observed depth of extinction of the shallow perturbations depends on their frequency in a manner that is consistent with the linear gravity wave theory (blue dotted curve in Fig. 3E). A frequency-wavenumber analysis (Fig. 2D) reveals that the signal is mainly composed of two dispersive wave trains, propagating landward and cross-shore with speeds decreasing from about 25 to 10 m/s. The dispersion curve associated with the strongest amplitudes is effectively explained by the dispersion relationship of the linear gravity wave theory (*18*):

$$\omega = \sqrt{g.k.tanh(k.h)}$$

where g is the acceleration of gravity and $\omega$ the frequency. For the comparison in Fig. 2D, the depth $h$ is fixed to 100 m, because this is the average depth for the first 8 km of the cable. The second dispersion curve appears to be similar to the first one but is compressed along the k-axis and therefore can be explained as a wave train impinging on the cable at a different angle, near $53^{0}$ degrees. Besides the two dominant wave trains, we detect a third signal propagating oceanward with much smaller amplitudes. Because its dispersion curve is symmetric to that of the main landward wavefield, we infer that it corresponds to a reflection off the coast. Its faint amplitudes are coherent with field experiments showing that most (>90%) of the sea-swell energy is dissipated in the surf zone (*19*). At depths greater than 100 m, the background amplitude becomes independent of depth (Fig. 2C) as predicted by the theory of second-order pressure fluctuation (*20*). Overall, the OF cable provides direct and continuous observations of seafloor perturbations due to the interaction between the shoaling bathymetry and the ocean waves (*21*) (Fig 2E and supplementary movie). This interaction is one of the major sources of micro-vibrations traveling through the solid earth, and is known as primary microseismic noise.

In the abyssal plain, below a depth of 2000 m, the background signal is dominated by two opposite wave trains propagating with similar dispersion properties (Fig. 3A,B). Compared to the continental shelf records, these higher frequency waves (mainly 0.2 to 0.8 Hz) propagate at speeds close to that of acoustic waves in water (1500 m/s), suggesting that they are Scholte waves, surface waves propagating along the seafloor interface (Fig. 3B). This interpretation is confirmed by simulations of the fundamental Scholte mode (*22*) using a regional 1D velocity model (*23*) (Fig. 3B). The speed of Scholte waves is mainly controlled by the velocity of the top sedimentary layer and changing the compressional value to 1500 or 2000 m/s is sufficient to explain the slight spreading of the dispersion curves (Fig. 3C). These waves are thought to result from the interaction of ocean waves propagating in opposite directions creating second-order pressure fluctuations. These fluctuations oscillate at double the ocean wave frequency and have been shown to couple into seismo-acoustic waves down to the seafloor(*20*). Indeed, the dominant frequency of the swell observed on the continental shelf is between 0.1 and 0.25 Hz (Fig 2D), while the dominant frequency observed in the abyssal plain is between 0.2 and 0.5 Hz (Fig 3E). This opposite wave interaction is the main contributor to the secondary microseismic peak identified in the noise spectrum of worldwide broadband seismic stations(*24*). The dominant frequency of the Scholte waves changes with depth as a result of the water column resonance effect that amplifies certain frequencies (Fig. 3D,E)(*21*).

The direct observation of these two major sources of seismic noise - wave-wave and wave-bathymetry interactions - demonstrates the potential of DAS to study the underlying physical processes and to quantify their spatio-temporal evolution. The dense monitoring of seafloor pressure fluctuations and interface seismic waves could also serve as a proxy to monitor the evolution of oceanic waves(*25*). The acoustic excitation of the seafloor caused by surface oceanic waves leads to the primary and secondary microseismic peaks in the noise spectrum. To our knowledge, this is the first time that the evolution of the ocean-solid earth interactions have been tracked continuously from the coast to the deep ocean.

The OF cable is also sensitive enough to detect local micro-earthquakes. The Toulon region is characterized by moderate seismic activity. Over the duration of the experiment, the regional seismic network detected several earthquakes with magnitudes between 1 and 2.3 (http://sismoazur.oca.eu/). The POSA broadband seismic station, part of the regional network, is located close to the cable landing site and provided reference measurements (Fig. 1). The largest event clearly recorded by the POSA station over the time period of the study was an earthquake of local magnitude 1.9 that occurred on February 20, 2018 at 05:31:32 UTM, north-east of the cable at a distance of 80 to 100 km (lat: 43.581°, lon: 6.635°, Fig. 1). The wavefield recorded by the OF is dominated by S- and surface waves, which is consistent with the POSA record in which the P-waves are barely visible on the vertical component, and not at all on the horizontal components (Fig. 4). The lack of P-wave observations on the OF is therefore due to wave attenuation and source radiation pattern, and not to a lack of OF sensitivity. Similar seismic phases were therefore observed with the OF and an on-land broadband station (Fig. S1).
On both sensors, the earthquake can be seen in the same frequency band, between 2 and 20 Hz (Fig. S1), and its signal is buried in noise at lower and higher frequencies. The noise spectrum also appears similar on both sensors. For such a small earthquake, the peak ground velocity in POSA only reaches 2 μm/s. Under the assumption of an incoming plane wave, strain can be multiplied by the apparent velocity (here 2155 m/s) and compared to the POSA ground velocity signal (*10*). This results in a signal twice as large, which is consistent with amplification by the presence of soft sediments on the seafloor (Fig. S1). Therefore, we find that the OF cable is able to record very small earthquakes with a sensitivity comparable to that of a broad-band seismic land station.

There was a significant variability in the amplitude of the recorded strain-rate along the entire cable length with two clear minima around km 8 and 14 (Fig. 4). These minima correspond to sections where the cable straddles canyons and probably does not directly lie on the seafloor, thus the coupling is poor. This interpretation would also explain the stronger coupling observed on the edges of the canyons where the cable has to support the extra weight of its neighboring sections. Alternatively, the sections of higher amplitude could correspond to site effects with amplification of the seismic wavefield at the bathymetry highs. Similarly, high amplitude signals from km 17 to 20 are likely related to “freely oscillating” portions of the OF in an area of steep and rough bathymetry. It is not clear which hypothesis to favor given the uncertainties on the exact location of the cable and on the morphology and composition of the seafloor. The weak signal observed between km 28 and 33 could be attributed to a local change in the cable orientation due to repair operations in 2017 but the stronger signal over small sections suggests that it is more likely due to a lower coupling, possibly related to the redeployment of the cable on top of the sediment cover following the repair operations. Beyond these different fluctuations, we notice a slight increase in the mean amplitude response of the cable, by about 15%, beyond km 18 (Fig. S3). This point corresponds to the transition from armored to non-armored cable structure. In summary, the signal quality and

ground coupling over the 41.5 km of cable seem to be mainly controlled by variations in the bathymetry and sediment cover, rather than changes in the cable structure: the transitions of the cable from double to simple armoring, or to lightweight protection are not associated with drastic changes in the quality of the recordings.

The results presented in this study demonstrate that DAS is directly applicable to seafloor telecommunication cables. Owing to its dense spatial and temporal sampling of seismo-acoustic signals, in the oceans and along their margins, DAS promises a wide spectrum of scientific and environmental applications. Here, we have presented records related to a small local earthquake, ocean surface gravity wave and microseismic noise, but the approach could be applied to the monitoring of many other sources of acoustic signals, such as those generated by mammals or marine traffic.

DAS is based on reflectometry, meaning that the signal analyzed is inherently weaker and has a shorter range than the direct signal. With small modifications, the repeaters installed all along the seafloor telecommunication cables could re-amplify the signal to reach greater distances and back-propagate to the source (Fig. S4). Yet, the standard range of 30 to 50 km is already enough to monitor active and passive margins, from the coast to the abyssal plains, thus encompassing most marine and geologic processes (e.g. subduction earthquakes, landslides, coastal erosion processes), including those of greater socio-economic concern.

DAS has several key advantages over transmission analysis: it only requires access to one end of the seafloor cable -transmission analysis would not have been possible on the MEUST-NUMerEnv cable- and it provides dense spatial sampling of the wavefield. This latter advantage enables an an additional range of applications, such as array techniques for detecting and tracking the sources of seismo-acoustic signals(*26*, *27*), reconstructing the water wave elevation(*28*), or passive imaging techniques to infer the internal structure of the ocean and of the Earth(*10*). Array techniques using communication cables that are already in place along subduction margins could allow near-field tracking of the seismic rupture and more effective seismic and tsunami early-warning systems(*29*). With the long lifetime of seafloor communication cables, typically designed to operate 25 years, imagery of the seafloor could be repeated over time to monitor changes in its properties, like those related to coastal erosion, fluid circulation or extraction. The long quest to monitor the dynamics of the seafloor beyond just a few sampling points now appears to be within reach.

## *Figures*

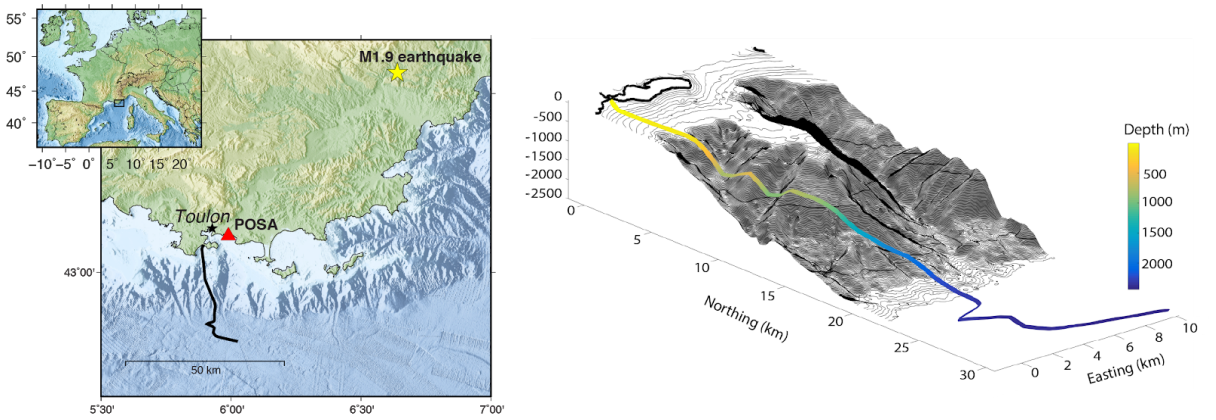


**Fig. 1**: **Map and perspective view of the seafloor MEUST-NUMerEnv cable**. The optic fibre cable offshore Toulon, France, shown in (a) map view and (b) 3D view. The 41.5 km long optical fiber crosses several oceanic domains : the shallow continental shelf, the steep continental slope and the deep oceanic plain. The yellow star on the map indicates the location of a magnitude 1.9 earthquake. The red triangle is the permanent seismic station POSA.

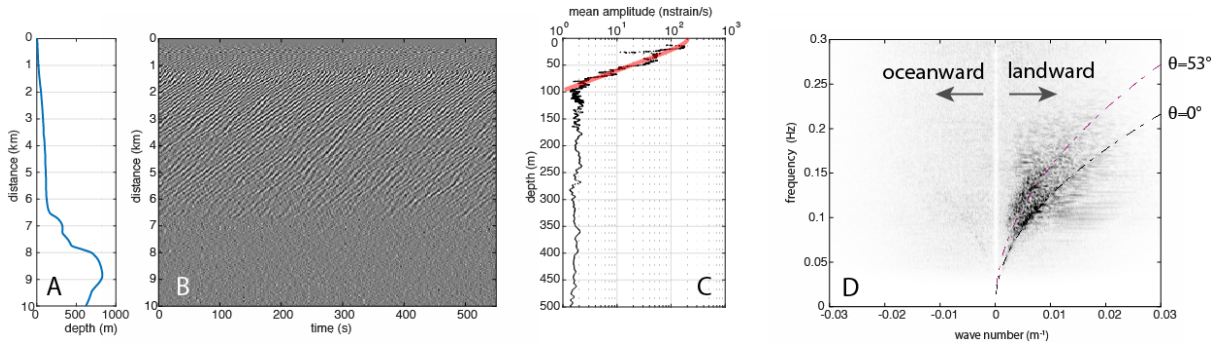


**Fig. 2. Seismic seafloor signal caused by oceanic surface gravity waves** (A) Depth profile and (B) 550 s long record of strain-rate along the first 10 km of the cable. Each trace is normalized by its maximum amplitude. The data shows periodic oscillations mainly propagating towards the shore. (C) Mean strain-rate over the same distance as a function of depth and theoretical prediction for intermediate depth regime and a wavelength of 100 m. (D) Frequency-wavenumber (f-k) decomposition of the strain-rate signal, for seaward (k<0) and landward (k>0) components, and linear gravity wave dispersion curves for two different incidence angles assuming a water depth of 100 m (dashed curves). (E) 3D perspective view on the strain-rate produced by the oceanic waves. The wavelength shrinks with decreasing water depth (see Movie in Supplementary material).

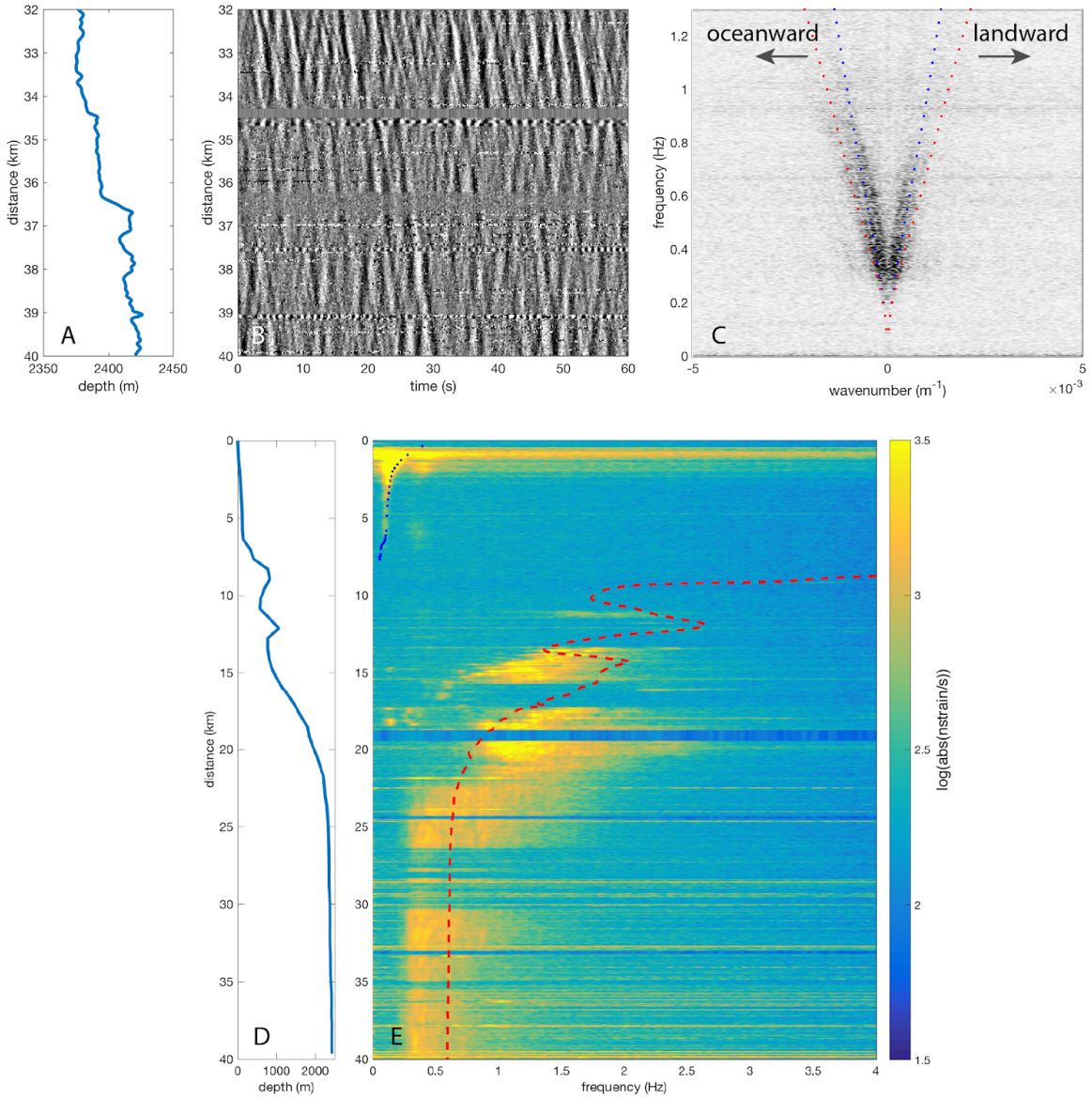


**Fig. 3. Observations of oceanic secondary microseismic noise.** (A) Depth profile of the OF cable. (B) 60 s record of strain-rate between km 32 and 40. (C) F-k decomposition of the signal. The dotted lines are the modeled frequencies of peak amplitude (minimum group velocity) of the fundamental mode of Scholte waves assuming the velocity model of (*23*) and varying the P-wave velocity in the top sedimentary layer (1500 m.s$^{-1}$ in red and 2000 m.s$^{-1}$ in blue). (D) Depth profile of the OF cable along its full length. (E) Spectrum of the noise along the cable. The pressure directly produced by the swell vanishes at a depth that depends on frequency as predicted by linear theory (blue dotted curve shows predicted depth of 95% amplitude loss). Beyond 8 km from the coast, at depths larger than 200 m, the OF cable senses the second-order pressure fluctuations caused by the sea surface waves. In deep water, the frequencies of maximum energy are consistent with those predicted from the water column resonance effect that amplifies the Scholte waves (red dashed curve).

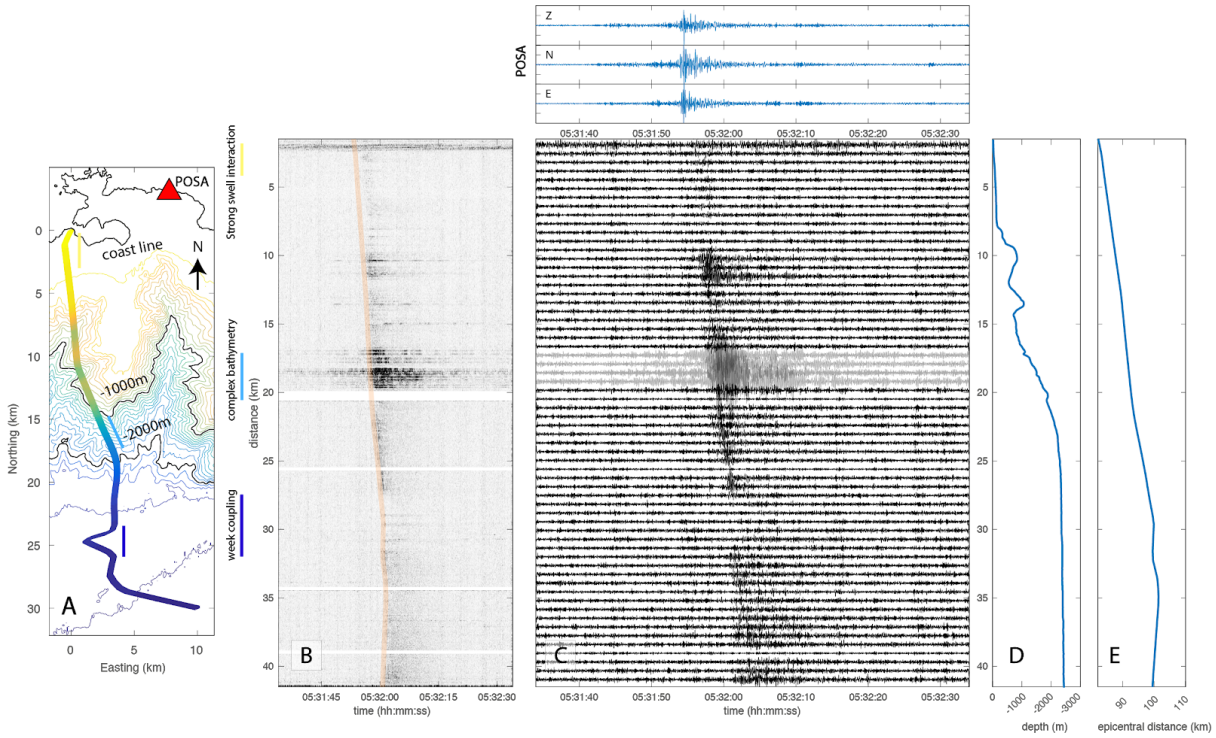


**Fig. 4. Comparison of the M1.9 earthquake recorded at land station POSA and along the fiber optic cable.** (A) Bathymetry map of the OF cable and location of the broad band land station POSA (red triangle). DAS data are plotted either as strain-rate absolute amplitude filtered between 1 and 15 Hz measured every 10 m (B), or as strain-rate averaged along 320 m sections of the cable (C). The shaded portion in (C) indicates the section of cable with high amplifications and where the OF cable crosses a complex bathymetry. On top are plotted for comparison the three-component records of station POSA. The two plots on the right side show the cable depth and epicentral distance at different distances along the cable.

**Supplementary Materials**

**Main characteristics of the MEUST-NUMerEnv cable**

The MEUST-NUMerEnv cable straddles several oceanic domains of the north Mediterranean margin: a shallow continental shelf, a steep continental slope (12% average slope), and a 2500 m-deep oceanic plain. Its armoring is adapted for the specific conditions for each domain and the associated risks of damage: Double Armoring Heavy (DAH) for the first 2.1 km, Single Armoring Heavy (SAH) for the next 15.1 km, and Light-Weight Protection (LWP) for the remaining 24 km. On land, an extra 1.4 km of fiber connects the cable to the shore station. From that shore station to the seafloor termination point of the cable, the OF remains of the same type (Corning LEAF©).

**Figures S1-S4**

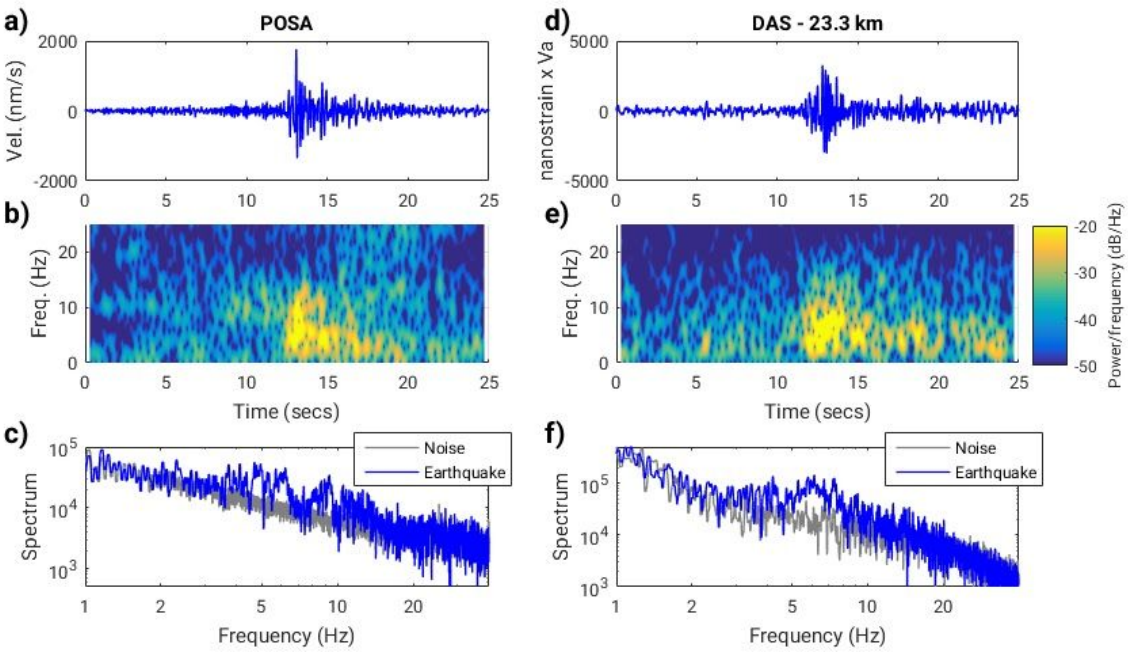


**Fig. S1: East-west velocity records of M1.9 earthquake at station POSA compared to strain OF measurements.** Comparison of a M1.9 earthquake recorded by the on-land station POSA (a, b,c) and by the OF cable at km 23.3 (d,e,f). a) and d) time signals are filtered between 2 and 20 Hz; b) and d) spectrograms of the signals filtered between 2 and 25 Hz; c) and f) spectrum of the earthquake (blue) and the noise (grey). The signals recorded on the optic fiber have been converted to strain through a time integration, and stacked with a normal moveout correction on a 384 m section. For comparison with the POSA velocity record, the signal was also multiplied by the apparent velocity (Va=2155 m/s), assuming that the record corresponds to an incoming plane wave.

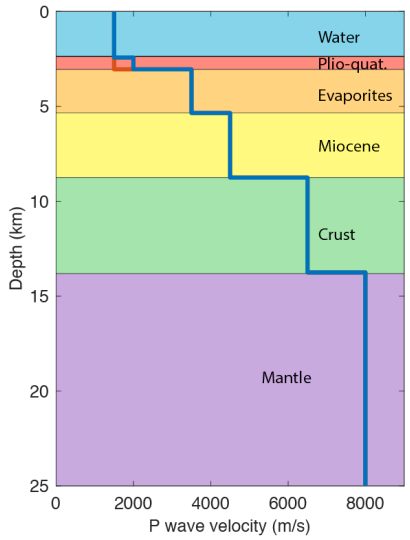


**Fig S2: P-wave seismic velocity model used to model the secondary microseismic noise.** Model derived from (*23*)

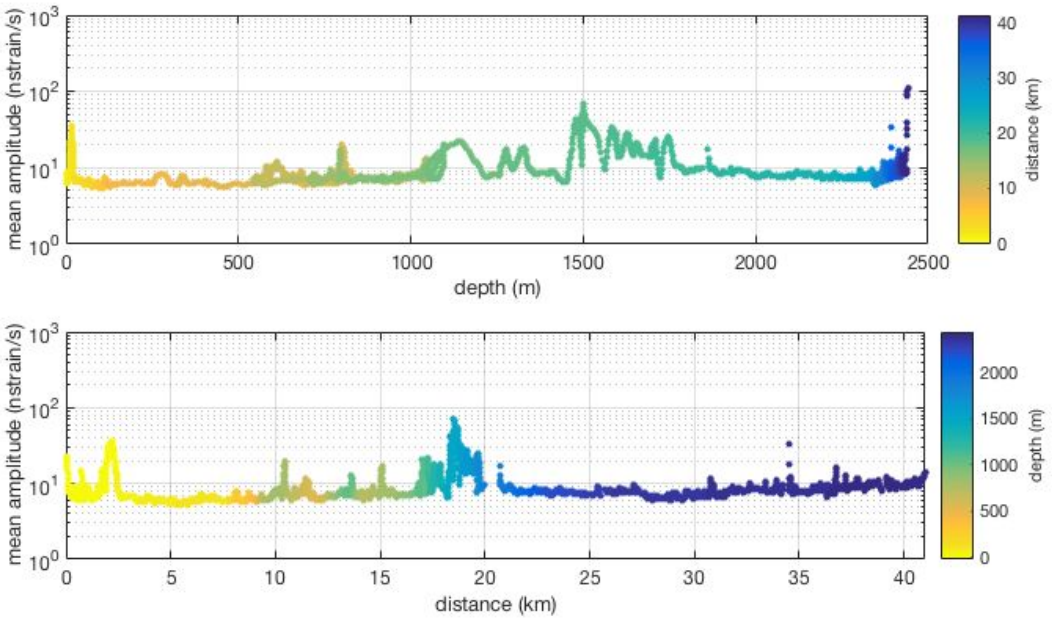


**Fig S3: Variations in the mean strain-rate during an earthquake.** Mean nano strain-rate amplitude as a function of depth (top) and distance (bottom) recorded during the magnitude 1.9 earthquake. The earthquake signal is filtered between 2.5 and 15Hz.

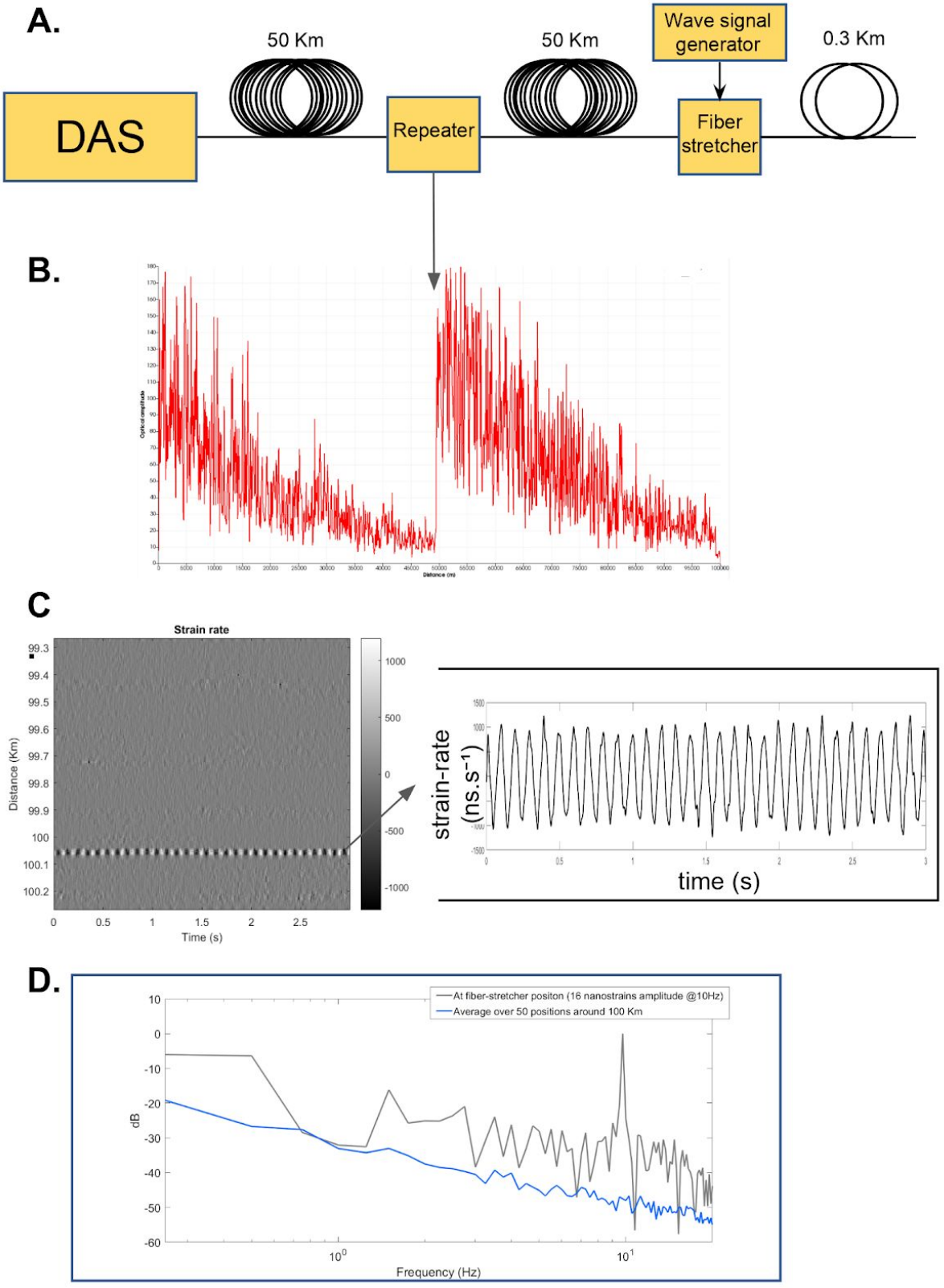


**Fig. S4: DAS measurement at 100km with repeater.** A) A standard DAS acquisition unit is connect to two 50 km fiber spools with a two-way optical repeater in between to re-amplify the signal. At the end of the fiber, a fiber stretcher applies controlled 16 nanostrain vibrations at 10Hz. B) Optical amplitude decay of the optical signal along the fiber. C) The strain-rate signal measured by the DAS unit at the location of the fiber stretcher. D) Spectrogram of

strain at the fiber-stretcher position (grey) or averaged at 50 points outside that area (blue). These figures demonstrate the ability to extend the range of a standard DAS unit without compromising the quality of the measurement.

**Movie S1: Seismic signal recorded over the continental shelf.** Perspective view of the bathymetry and the first 8km of seafloor cable. The movie presents one minute of evolution of the amplitude of the seismic signal. The amplitude fluctuations illustrate the motion of the vertical pressure exerted by ocean surface waves propagating at the surface. These wave propagate predominantly towards the shore with a wavelength controlled by the water depth.

## References


1. G. Nolet *et al.*, Imaging the Galápagos mantle plume with an unconventional application of floating seismometers. *Sci. Rep.* **9** (2019), doi:10.1038/s41598-018-36835-w.
2. S. C. Riser *et al.*, Fifteen years of ocean observations with the global Argo array. *Nat. Clim. Change*. **6**, 145–153 (2016).
3. P. Favali, L. Beranzoli, A. D. Santis, *SEAFLOOR OBSERVATORIES: A New Vision of the Earth from the Abyss* (Springer Science & Business Media, 2015).
4. E. Kintisch, Cut hardware to save ocean science, says National Academies panel. *Sci. AAAS* (2015), (available at http://www.sciencemag.org/news/2015/01/cut-hardware-save-ocean-science-says-national-academies-panel).
5. D. A. Walker, Using transoceanic cables to quantify global environmental changes. *Eos Trans. Am. Geophys. Union*. **72**, 393–398 (1991).
6. F. Tilmann, B. M. Howe, R. Butler, Commercial underwater cable systems could reduce disaster impact. *Eos Trans AGU*. **98** (2017).
7. G. Marra *et al.*, Ultrastable laser interferometry for earthquake detection with terrestrial and submarine cables. *Science*. **361**, 486–490 (2018).
8. A. H. Hartog, *An Introduction to Distributed Optical Fibre Sensors* (CRC Press, 2017; http://www.taylorfrancis.com/books/9781482259582).
9. N. J. Lindsey *et al.*, *Geophys. Res. Lett.*, in press, doi:10.1002/2017GL075722.
10. C. Yu, Z. Zhan, N. J. Lindsey, J. B. Ajo-Franklin, M. Robertson, The potential of distributed acoustic sensing (DAS) in teleseismic studies: insights from the Goldstone experiment. *Geophys. Res. Lett.* (2019), doi:10.1029/2018GL081195.
11. P. Jousset *et al.*, Dynamic strain determination using fibre-optic cables allows imaging of seismological and structural features. *Nat. Commun.* **9** (2018), doi:10.1038/s41467-018-04860-y.
12. J. B. Ajo-Franklin *et al.*, Distributed Acoustic Sensing Using Dark Fiber for Near-Surface Characterization and Broadband Seismic Event Detection. *Sci. Rep.* **9** (2019), doi:10.1038/s41598-018-36675-8.
13. A. D. Chave, G. Waterworth, A. R. Maffei, G. Massion, Cabled Ocean Observatory Systems. *Mar. Technol. Soc. J.* **38**, 30–43 (2004).
14. P. Lamare, The MEUST deep sea infrastructure in the Toulon site. *EPJ Web Conf.* **116**,

09001 (2016).
15. P. Coyle, KM3NeT Collaboration, KM3NeT-ORCA: Oscillation Research with Cosmics in the Abyss. *J. Phys. Conf. Ser.* **888**, 012024 (2017).
16. C. Vallee *et al.*, in *OCEANS 2015 - Genova* (IEEE, Genova, Italy, 2015; http://ieeexplore.ieee.org/document/7271335/), pp. 1–6.
17. R. Posey, G. A. Johnson, S. T. Vohra, Strain sensing based on coherent Rayleigh scattering in an optical fibre. *Electron. Lett.* **36**, 1688 (2000).
18. H. Lamb, Hydrodynamics Dover Publications. *N. Y.* (1945).
19. S. Elgar, T. H. C. Herbers, R. T. Guza, Reflection of Ocean Surface Gravity Waves from a Natural Beach. *J. Phys. Oceanogr.* **24**, 1503–1511 (1994).
20. M. S. Longuet-Higgins, A Theory of the Origin of Microseisms. *Philos. Trans. R. Soc. Lond. Ser. Math. Phys. Sci.* **243**, 1–35 (1950).
21. K. Hasselmann, A statistical analysis of the generation of microseisms. *Rev. Geophys.* **1**, 177 (1963).
22. M. M. Haney, V. C. Tsai, Perturbational and nonperturbational inversion of Rayleigh-wave velocities. *Geophysics*. **82**, F15–F28 (2017).
23. J.-X. Dessa *et al.*, The GROSMarin experiment: three dimensional crustal structure of the North Ligurian margin from refraction tomography and preliminary analysis of microseismic measurements. *Bull. Soc. Geol. Fr.* **182**, 305–321 (2011).
24. E. Stutzmann, M. Schimmel, G. Patau, A. Maggi, *Geochem. Geophys. Geosystems*, in press, doi:10.1029/2009GC002619.
25. F. Ardhuin, A. Balanche, E. Stutzmann, M. Obrebski, *J. Geophys. Res. Oceans*, in press, doi:10.1029/2011JC007449.
26. L. Meng, J.-P. Ampuero, A. Sladen, H. Rendon, High-resolution backprojection at regional distance: Application to the Haiti M7.0 earthquake and comparisons with finite source studies. *J. Geophys. Res.* **117**, B04313 (2012).
27. L. De Barros, A. Deschamps, A. Sladen, H. Lyon-Caen, N. Voulgaris, *Geophys. Res. Lett.*, in press, doi:10.1002/2017GL075460.
28. P. Bonneton, D. Lannes, Recovering water wave elevation from pressure measurements. *J. Fluid Mech.* **833**, 399–429 (2017).
29. L. Meng, R. M. Allen, J.-P. Ampuero, Application of Seismic Array Processing to Earthquake Early Warning. *Bull. Seismol. Soc. Am.* **104**, 2553–2561 (2014).

**Acknowledgements**

We thank the team from the Centre de Physique des Particules de Marseille who greatly facilitated the access the infrastructure. The MEUST infrastructure is financed with the support of the CNRS/IN2P3, the Region Sud, France (CPER the State (DRRT) and the Europe (FEDER). This work was supported by the SEAFOOD project, funded in part by grant ANR-17-CE04-0007 of the French Agence Nationale de la Recherche and in part by Université Côte d'Azur IDEX program UCA$^{JEDI}$ ANR-15-IDEX-0001.